OPEN

Light: Science & Applications (2017) 6, e16259; doi:10.1038/lsa.2016.259
Official journal of the CIOMP 2047-7538/17
www.nature.com/lsa

ORIGINAL ARTICLE

# Generation of wavelength-independent subwavelength Bessel beams using metasurfaces

Wei Ting Chen[1], Mohammadreza Khorasaninejad[1], Alexander Y. Zhu[1], Jaewon Oh[1,2], Robert C. Devlin[1], Aun Zaidi[1] and Federico Capasso[1]

**Bessel beams are of great interest due to their unique non-diffractive properties. Using a conical prism or an objective paired with an annular aperture are two typical approaches for generating zeroth-order Bessel beams. However, the former approach has a limited numerical aperture (NA), and the latter suffers from low efficiency, as most of the incident light is blocked by the aperture. Furthermore, an additional phase-modulating element is needed to generate higher-order Bessel beams, which in turn adds complexity and bulkiness to the system. We overcome these problems using dielectric metasurfaces to realize meta-axicons with additional functionalities not achievable with conventional means. We demonstrate meta-axicons with high NA up to 0.9 capable of generating Bessel beams with full width at half maximum about as small as ~$\lambda$/3 ($\lambda = 405$ nm). Importantly, these Bessel beams have transverse intensity profiles independent of wavelength across the visible spectrum. These meta-axicons can enable advanced research and applications related to Bessel beams, such as laser fabrication, imaging and optical manipulation.**
*Light: Science & Applications* (2017) **6,** e16259; doi:10.1038/lsa.2016.259; published online 19 May 2017

**Keywords:** Bessel beam; high numerical aperture; light angular momentum; metasurface

## INTRODUCTION

Non-diffracting Bessel beams are a set of solutions of the free space Helmholtz equation and have transverse intensity profiles that can be described by the Bessel functions of the first kind. Since their discovery in 1987[1], they have exhibited many interesting properties such as non-diffraction[1], self-reconstruction[2] and even providing optical pulling forces[3,4]. The scalar form of Bessel beams propagating along the $z$ axis can be described in cylindrical coordinates ($r$,$\phi$,$z$) by:

$$E(r,\phi,z) = A \cdot \exp(ik_z z) \cdot J_n(k_r r) \cdot \exp(\pm in\phi) \quad (1)$$

where $A$ is the amplitude, $k_z$ and $k_r$ are the corresponding longitudinal and transverse wavevectors that satisfy the equation $\sqrt{k_z^2 + k_r^2} = k = \frac{2\pi}{\lambda}$ (where $\lambda$ is the wavelength). Equation (1) shows that the transverse intensity profiles of Bessel beams are independent of the $z$ coordinate, which gives rise to their non-diffracting characteristic. It also indicates that any higher-ordered Bessel beam ($n \neq 0$) must carry orbital momentum and have zero intensity along the $z$ axis at $r = 0$ because of the phase singularity resulting from the $\exp(\pm in\phi)$ term.

Ideal Bessel beams are not spatially limited and carry infinite energy; therefore, they can only be approximated within a finite region by the superposition of multiple plane waves. This can be achieved by symmetrically refracting incident plane waves toward the optical axis of a conical prism, an axicon, to generate a $J_0$ Bessel beam. Figure 1a shows the schematic diagram of a conventional axicon. The numerical aperture (NA) of an axicon is related to the angle $\alpha$ (Figure 1a) by:

$$\mathrm{NA} \equiv \sin(\theta) = \sin\left(\sin^{-1}(n \cdot \sin(\alpha)) - \alpha\right) \quad (2)$$

where $n$ is the refractive index of the constituent material, often glass. This equation and Figure 1a show that for a given refractive index, achieving high NA axicons requires an increase in $\alpha$. Considering a refractive index of 1.5, typical of most silica glasses, total internal reflection occurs when $\alpha > 42°$. Thus, the NA of a conventional axicon cannot exceed 0.75 (Supplementary Fig. S1). This, in turn, also limits the minimum achievable full width at half maximum (FWHM) of the Bessel beam. In addition, the tip of a refractive axicon is rounded instead of being perfectly sharp because of limitations in glass polishing, which again affects the FWHM of the Bessel beam[5]. Herein, the FWHM of the zeroth-order Bessel beam $J_0$ is defined as the distance between two points at half of the maxima intensity of the center bright spot, and can be derived from Equation (1) as:

$$\mathrm{FWHM}_{J_0} = \frac{2.25}{k_r} = \frac{0.358\lambda}{\mathrm{NA}} \quad (3)$$

where $k_r = \frac{2\pi}{\lambda} \cdot \mathrm{NA}$. Similarly, the FWHM of a $J_1$ Bessel beam is defined as twice the distance from the dark spot center to the point at its closest ring with the half maxima intensity, and given by:

$$\mathrm{FWHM}_{J_1} = \frac{1.832}{k_r} = \frac{0.292\lambda}{\mathrm{NA}} \quad (4)$$

[1]Harvard John A. Paulson School of Engineering and Applied Sciences, Harvard University, Cambridge, MA 02138, USA and [2]University of Waterloo, Waterloo, ON N2L 3G1, Canada
Correspondence: F Capasso, Email: capasso@seas.harvard.edu
Received 3 August 2016; revised 25 November 2016; accepted 26 November 2016; accepted article preview online 3 December 2016

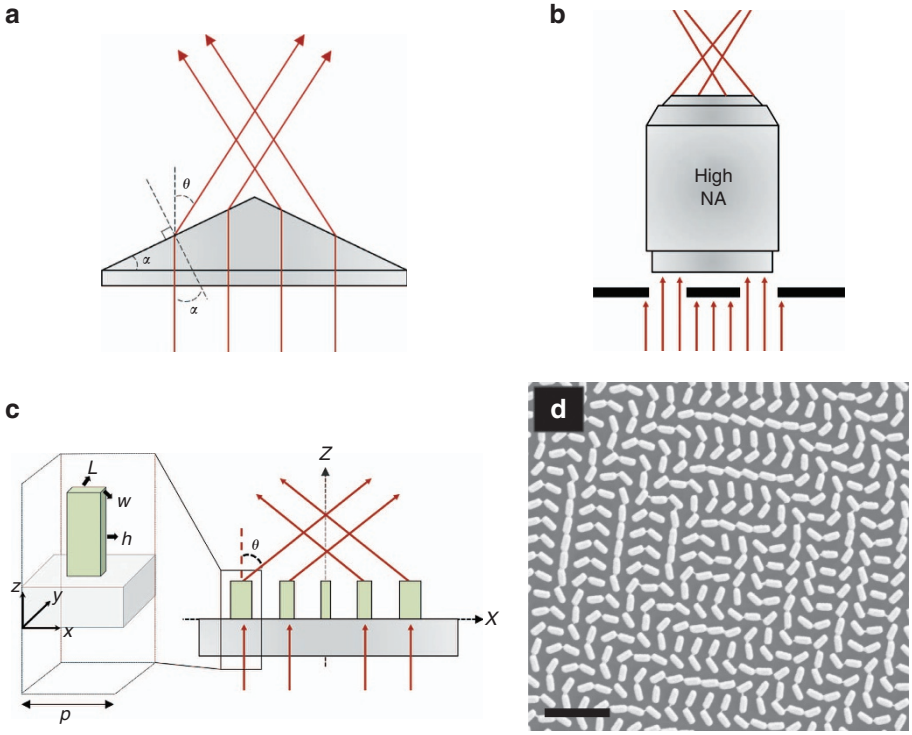


**Figure 1** Comparison of conventional axicons with meta-axicon. (**a**, **b**) Schematic diagram of two conventional approaches for generating a $J_0$ Bessel beam. (**a**) Cross-section of a conventional refractive axicon comprised of a glass prism. The axicon angle $\alpha$ and the refraction angle $\theta$, which determine the NA, are labeled. (**b**) A high NA objective paired with an annular aperture for generating a $J_0$ Bessel beam. (**c**) Schematic diagram of a meta-axicon. The meta-axicon deflects an incident collimated light to an angle $\theta$ toward its center to generate Bessel beams. The meta-axicon is composed of identical $TiO_2$ nano-fins but different rotation angle $\theta_{nf}$ with respect to its geometrical center. Two different meta-axicons with NAs of 0.9 and 0.7 are designed at wavelengths $\lambda = 405$ and 532 nm with corresponding dimensions ($L = 125$ nm, $W = 60$ nm, $h = 600$ nm, $P = 155$ nm) and ($L = 210$ nm, $W = 65$ nm, $h = 600$ nm, $p = 250$ nm). (**d**) A scanning electron microscope micrograph of a fabricated meta-axicon. Scale bar = 1 μm.

In the case of conventional axicons, the NA is almost constant within the visible region due to the weak dispersion of glass. Thus, the FWHM of the $J_0$ beam is proportional to wavelength and varies accordingly. For example, changing the wavelength from 400 to 700 nm can result in a difference of 175% in the FWHM. Alternatively, a high NA objective lens paired with an annular aperture is usually used to generate Bessel beams with subwavelength FWHMs[6], as shown in Figure 1b. However, this configuration is not efficient as most of the incident light is blocked by the aperture. Both methods require the addition of phase-modulating elements, such as spatial light modulators or spiral phase plates, to generate higher-ordered Bessel beams.

In recent years, metasurfaces, consisting of subwavelength-spaced phase shifters, have been demonstrated to fully control the optical wavefront[7–12]. Various compact optical components have been reported including lenses[13–17], holograms[18–21], modulators[22–24] and polarization-selective devices[25–28]. Metallic and dielectric metasurface axicons were reported in Ref. 29 and Ref. 27, respectively; both had low NAs. Unlike conventional phase-modulating devices (for example, spatial light modulators), metasurface-based devices can provide subwavelength spatial resolution, which is essential in order to deflect light by very large angles. This is mandatory to realize high NA optical components, including axicons and lenses capable of generating beams with even smaller FWHM. Various applications, including (but not limited to) scanning microscopy[6,30,31], optical manipulation[32–34] and lithography[35,36], all require subwavelength FWHM to achieve high spatial resolution, strong trapping force and subwavelength feature sizes, respectively. Here we report meta-axicons with high NA up to 0.9 in the visible region that are capable of generating, not only the zeroth-order, but also higher-ordered Bessel beams with FWHM about one-third of the wavelength without the use of additional phase elements. In addition, by appropriately designing the metasurfaces' phase shifters, the transverse field intensity profiles are maintained independent of the wavelength.

## MATERIALS AND METHODS

Figure 1c shows a schematic diagram of a meta-axicon. The basic elements of the meta-axicon are identical rotated titanium dioxide ($TiO_2$) nano-fins with height $h$, length $L$ and width $w$, arranged in a square lattice. To maximize the performance of the meta-axicon, each nano-fin should act as a half-waveplate at the design wavelength, converting incident circularly polarized light to its orthogonal polarization state. To tailor the required phase profiles, we use geometric phase associated with the rotation angle of the nano-fin, known as the Pancharatnam–Berry phase[37,38]. The $h$, $L$ and $w$ parameters are determined using the three-dimensional finite difference time domain (FDTD from Lumerical Inc.) method to maximize the circular polarization conversion efficiency[39,40]. At the design wavelength $\lambda_d = 405$ nm, simulated polarization conversion efficiencies $> 90\%$ were obtained. The efficiencies decrease as NA increases due to the sampling criterion (Supplementary Fig. S2). To determine the polarization conversion efficiency, we arranged an array of $TiO_2$ nano-fins in such a way to deflect light to a particular angle and then the efficiency is calculated by dividing the total deflected optical power by


doi:10.1038/lsa.2016.259

the input optical power. Perfectly matched layer boundary conditions were used normal to the propagation of the incident circularly polarized light and periodic conditions were used for the remaining boundaries.

For the generation of a zeroth-order Bessel beam, a meta-axicon requires a radial phase profile $\varphi(r)$ with a phase gradient

$$\frac{\mathrm{d}\varphi}{\mathrm{d}r} = -\frac{2\pi}{\lambda_\mathrm{d}}\sin(\theta) \tag{5}$$

This can be understood from the generalized Snell's law[9] as the condition for all light rays to be refracted by the same angle $\theta$ at the design wavelength $\lambda_\mathrm{d}$, where $\sin(\theta)$ is the NA. Integrating Equation (5) gives:

$$\varphi(x,y) = 2\pi - \frac{2\pi}{\lambda_\mathrm{d}}\cdot\sqrt{x^2+y^2}\cdot\mathrm{NA} \tag{6}$$

where $\sqrt{x^2+y^2} = r$. The generation of the high-order Bessel beams requires the addition of a term $n\phi$, where $\phi = \mathrm{atan}(\frac{y}{x})$ is the azimuthal angle, which represents the phase of an optical vortex imparted to the deflected light. Equation (6) then becomes

$$\varphi(x,y) = 2\pi - \frac{2\pi}{\lambda_\mathrm{d}}\cdot\sqrt{x^2+y^2}\cdot\mathrm{NA} + n\phi \tag{7}$$

This phase profile is imparted by the rotation of each nano-fin at a position $(x, y)$ by an angle $\theta_{nf}(x,y) = \frac{\varphi(x,y)}{2}$ for the case of left-handed polarized incidence. $TiO_2$-based meta-axicons are fabricated using the approach described in Ref.41, which can prevent tapered sidewall[42]. Figure 1d shows a scanning electron microscope image of the center part of a fabricated meta-axicon. We used a custom-built microscope to characterize the meta-axicons. A schematic diagram of the set-up and the optical components used can be found in Supplementary Fig. S3.

## RESULTS AND DISCUSSION

Figure 2a and 2d shows the measured transverse intensity profile of the $J_0$ and $J_1$ Bessel beams at $\lambda = 405$ nm, whereas Figure 2b and 2e shows the intensity along a horizontal cut across the centers of Figure 2a and 2d, respectively. The measured FWHM of the $J_0$ Bessel beam is observed to be ~163 nm with 3.5 nm standard deviation, which is very close to its theoretical limit of 160 nm (Equation (3)). The measured FWHM of the $J_1$ Bessel beam is 130 nm with 1.75 nm standard deviation, which agrees well with its theoretical value of 131 nm (Equation (4)). Figure 2c and 2f shows the intensity profile along the beam propagation direction of the $J_0$ and $J_1$ Bessel beams. Their FWHMs at different planes normal to the propagation $z$ axis are provided in Supplementary Fig. S4. Both the $J_0$ and $J_1$ Bessel beam have a depth of focus of 75 μm (150$\lambda$). This value is close to the theoretical value using geometric optics, that is, $\frac{D}{2\tan(\mathrm{asin(NA)})} = 72$ μm, where $D = 300$ μm is the diameter of the meta-axicons.

Polarization properties of a Bessel beam generated by a high NA meta-axicon can be very different from that of a corresponding axicon with low NA[43,44]. In order to understand the polarization properties of the $J_0$ and $J_1$ Bessel beams generated by the meta-axicons with NA = 0.9, we show in Figure 3 their theoretical (first row) and simulated (second row) normalized electric field intensities $|Ex|^2$, $|Ey|^2$ and $|Ez|^2$. Only a portion of the meta-axicon (30 μm in diameter), but with the same NA, was simulated due to limited computational

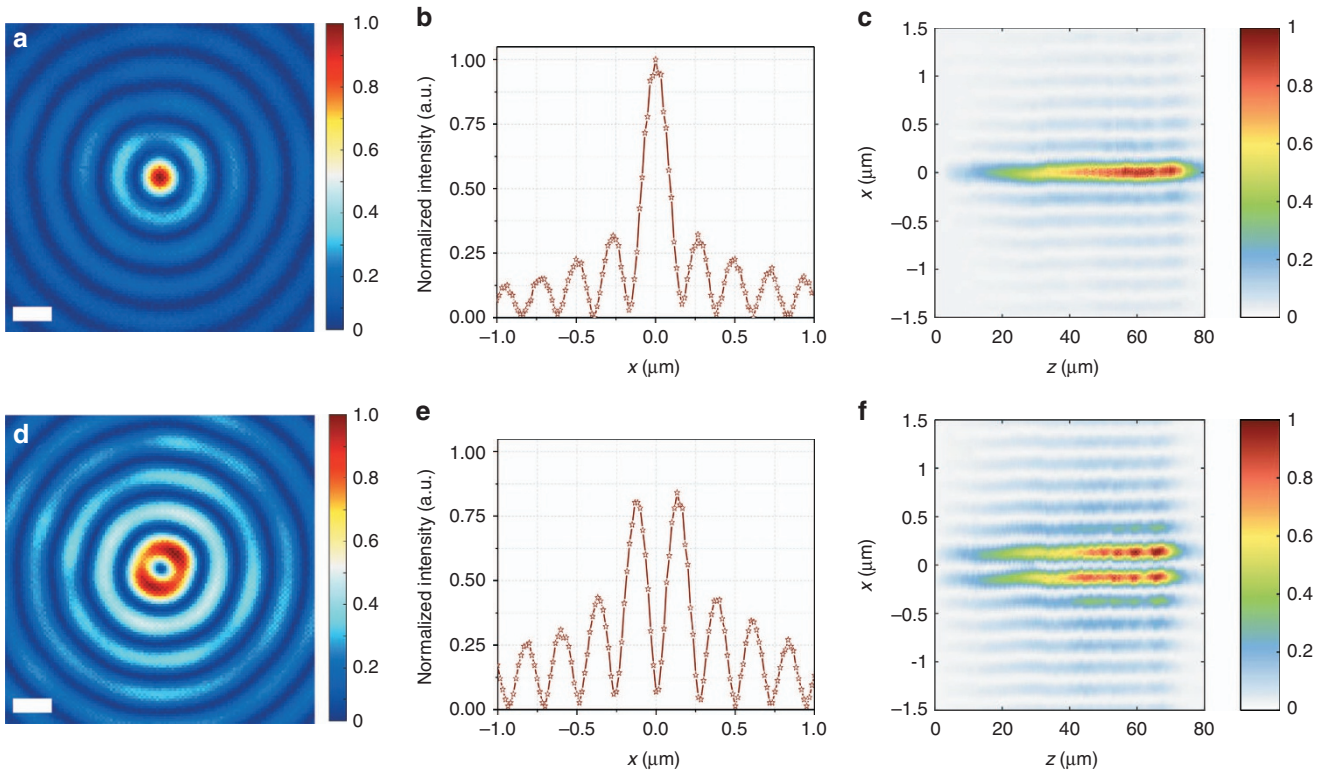


**Figure 2** Optical characterization of meta-axicons with NA = 0.9 designed at wavelength $\lambda_\mathrm{d} = 405$ nm. (**a**, **b**) Measured intensity profile (**a**) for the meta-axicon designed to generate $J_0$ (scale bar = 250 nm) and its corresponding horizontal cut (**b**). (**c**) Normalized intensity profile of the Bessel beam ($J_0$) along the propagation direction. (**d**, **e**) Measured intensity profile (**d**) for the meta-axicon designed to generate $J_1$ (scale bar = 250 nm) and its corresponding horizontal cut (**e**). (**f**) Normalized intensity profile of the Bessel beam ($J_1$) along the propagation direction.

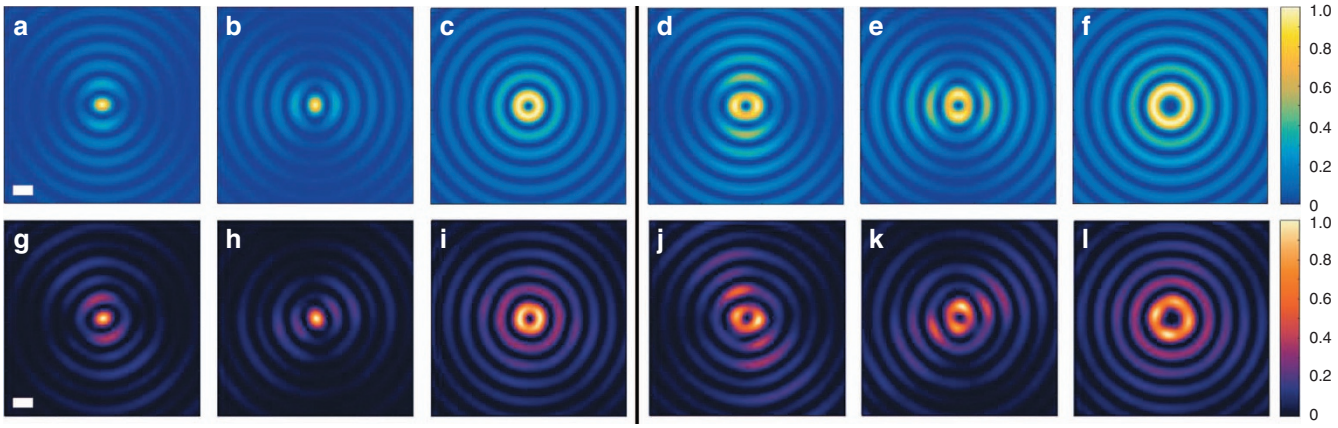


**Figure 3** Polarization properties of meta-axicons with NA = 0.9 designed at wavelength $\lambda_d = 405$ nm. A comparison of the square of the electric fields from theoretical calculation using Equation (8) (first row) and FDTD simulations (second row). The first (**a**, **g**), second (**b**, **h**) and third columns (**c**, **i**) show $|Ex|^2$, $|Ey|^2$ and $|Ez|^2$ for the $J_0$ Bessel beam, respectively. The corresponding plots for the $J_1$ Bessel beam are shown on the right side of the black line. Scale bar = 250 nm.

resources. A slight deviation of the simulations from theory results from the uncoupled light of nano-fins and the effects of the boundary in the simulations. We note that for either $|Ex|^2$ (Figure 3a and 3d) or $|Ey|^2$ (Figure 3b and 3e), the shape of the $J_0$ and $J_1$ Bessel beams at their respective centers is elliptical rather than circular. For example, as shown in Figure 3d and 3e, for $J_1$, the center regions are accompanied by two brighter spots at the end of the long axis of the ellipse. Moreover, the intensity of $|Ex|^2$ and $|Ey|^2$ show variation on their side lobes. These are also observed in their corresponding simulation results (Figure 3j and 3k). In addition, $|Ez|^2$ is described by a Bessel function one order larger than its transverse electric field. These properties can be explained by considering the vector form of Bessel beams. The theoretical vector solutions of the electric field of a Bessel beam propagating along the $z$ direction in cylindrical coordinates are:

$$\vec{E}(r,\phi,z) = E_0 \cdot e^{ik_z z} e^{i(n+1)\phi} \begin{pmatrix} (-C_{TE}\frac{J_n(k_r r)+J_{n+2}(k_r r)}{2} + i \cdot C_{TM} e^{i\eta}\sqrt{1-NA^2}\frac{J_n(k_r r)-J_{n+2}(k_r r)}{2})\hat{r} \\ -(C_{TM} e^{i\eta}\sqrt{1-NA^2}\frac{J_n(k_r r)+J_{n+2}(k_r r)}{2} + i \cdot C_{TE}\frac{J_n(k_r r)-J_{n+2}(k_r r)}{2})\hat{\phi} \\ NA \cdot C_{TM} e^{i\eta} J_{n+1}(k_r r)\hat{z} \end{pmatrix} \quad (8)$$

where $C_{TM}$ and $C_{TE}$ are complex numbers associated with the constituent transverse magnetic (TM) and transverse electric (TE) waves of Bessel beams, and $\eta$ is the phase difference between $C_{TM}$ and $C_{TE}$[3,45]). For our case (circularly polarized Bessel beams), $C_{TE}$ is equal to $C_{TM}$, $\eta = \pm\frac{\pi}{2}$, NA = 0.9, and $n = 0$ and $n = 1$ for $J_0$ and $J_1$ Bessel beam, respectively. For high NA Bessel beams, the electric field of the $z$ component results from TM waves: the higher the NA, the higher the contribution the TM waves make to $E_z$. The $E_r$ and $E_\phi$ components mainly result from TE wave contribution, as the term $\sqrt{1-NA^2}$ is relatively small for the high NA case. The term $\frac{J_n(k_r r)+J_{n+2}(k_r r)}{2}$ contributes to localized intensity near the center spot or the most inner ring, as $J_n(k_r r) \approx \sqrt{\frac{2}{\pi r}}\cos(r - \frac{n\pi}{2})$ for large $r$, such that $J_n(k_r r)$ and $J_{n+2}(k_r r)$ cancel each other due to a $\pi$ phase difference. The intensity distribution of side lobes away from the center of a Bessel beam is due to another term $\frac{J_n(k_r r)-J_{n+2}(k_r r)}{2}$. When we transform cylindrical $(r,\phi)$ to Cartesian coordinates $(x,y)$ using $\vec{E}_x = E_r \cdot \cos(\phi) - E_\phi \cdot \sin(\phi)$, we will have $\cos(\phi)$ modulation resulting in the elliptical center, and a corresponding modulation of $\sin(\phi)$ for the side lobe, which is shown in Figure 3a and 3d, respectively. This is a signature feature of high NA Bessel beams (see a comparison with a lower NA in Supplementary Fig. S5). Due to the spatially varying intensity of $E_x$ and $E_y$, the Bessel beams for high NA are not homogeneously polarized, but rather show space-variant polarization states (see Supplementary Fig. S6 for plots of ellipticity and polarization orientation angle). Therefore, only the center part of the $J_0$ Bessel beam can be circularly polarized in the case of high NA case.

By the judicious design of our metasurface, we compensate the wavelength dependency of the FWHM of Bessel beams (Equations (3) and (4)). As mentioned previously, the transverse intensity profile is determined by the factor $k_r = \frac{2\pi}{\lambda} \cdot NA$. In our case, the $NA = \frac{\lambda}{2\pi}\nabla\varphi(x,y,\lambda)$, where $\varphi$ follows Equation (7). Therefore, $k_r$ only depends on the phase gradient $\nabla\phi(x,y,\lambda)$, which can be designed to be wavelength-independent using the Pancharatnam–Berry phase concept. In this case, the phase gradient is a constant, and the NA is only proportional to the wavelength $\lambda$. This manifests experimentally, in the form of the increasing ring diameters in the Fourier plane of the meta-axicons for increasing wavelength (Supplementary Fig. S7). To demonstrate this unique characteristic across a broad wavelength region, we use the same method to design two meta-axicons for $J_0$ and $J_1$ with the NA = 0.7 at the wavelength $\lambda = 532$ nm. Each nano-fin ($L = 210$ nm, $W = 65$ nm and $h = 600$ nm) for this case is arranged in a square lattice, with a lattice constant of 250 nm. We show in Figure 4a–4d and 4f–4i the corresponding $J_0$ and $J_1$ Bessel beams in false color for different wavelengths (at $\lambda = 480$, 530, 590 and 660 nm) with a bandwidth of 5 nm at the $z$ plane about 60 μm away from the surface of meta-axicons. Note that the efficiency of the meta-axicon is dependent on wavelength. The efficiency was measured and is shown in Supplementary Fig. S8. The $FWHM_{J_0}$ and $FWHM_{J_1}$ for each wavelength spanning 470–680 nm are shown in Supplementary Fig. S9. Figure 4 explicitly indicates that the intensity profile for different wavelengths vary weakly, confirming wavelength-independent behavior. It is notable that for these measurements the distance between the meta-axicon and objective lens was kept unchanged. We also repeated the measurements using a supercontinuum laser of bandwidth 200 nm centered at 575 nm (see Supplementary Fig. S10 for its spectrum). The intensity profiles (Figure 4e and 4j) for both $J_0$ and $J_1$ remarkably changed weakly. It is important to note that in order to generate high NA and wavelength-independent Bessel beams, the Nyquist sampling theorem


doi:10.1038/lsa.2016.259

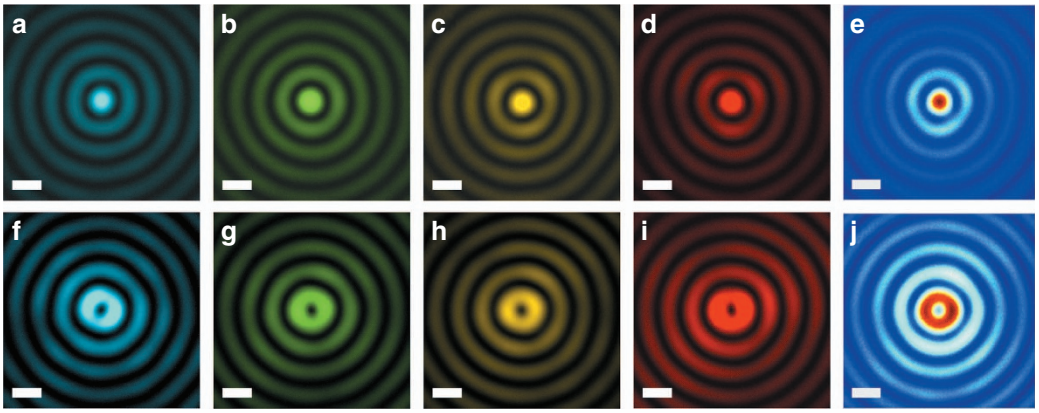


**Figure 4** Meta-axicons with wavelength-independent intensity profile. Two meta-axicons for $J_0$ (top row) and $J_1$ (bottom row) Bessel beams with NA = 0.7 designed at the wavelength $\lambda = 532$ nm were measured. (**a**–**d**, **f**–**i**) Measured intensity profiles at wavelengths $\lambda = 480$, 530, 590 and 660 nm, respectively. Intensity profiles are false colored for ease of visualization. (**e**, **j**) $J_0$ (**e**) and $J_1$ (**j**) intensity profiles measured using a tunable laser with center wavelength of 575 nm and a bandwidth of 200 nm. Besides changing the exposure time of the camera to avoid saturation, these images were taken without adjusting any other optical component, including the distance between the meta-axicon and objective, which were unchanged throughout the entire measurements. Scale bar = 500 nm.

and wavelength-independent phase gradient conditions both need to be satisfied. According to the Nyquist sampling theorem, one needs to sample the phase profile given by Equation (7) in the spatial domain with a rate that is at least twice the highest transverse spatial frequency. This requires the size of the unit cell to be equal to or smaller than $\frac{\lambda}{2 \cdot \mathrm{NA}}$, which cannot be satisfied by conventional diffractive elements. For example, spatial light modulators usually have ~6 μm pixel sizes[46] and photo-aligned liquid crystal devices are usually limited to a phase gradient of $\sim \pi/\mu$m[47], corresponding to a maximum achievable NA of about 0.03 and 0.26 in the visible region, respectively. It is also important to note that the phase profile of metasurfaces can also be designed by varying the geometrical sizes (length, width or diameter and so on) of the nanostructures, pixel by pixel[7,9]. However, these metasurfaces, not designed by the Pancharatnam–Berry phase, are accompanied by strong amplitude differences between each pixel at wavelengths away from the design wavelength. This becomes more significant within the absorption region of the constituent materials used. In addition, the unwanted amplitude difference between each pixel can result in the deflection of light to multiple angles[48], changing the profile of the Bessel beams. Utilizing the Pancharatnam–Berry phase approach minimizes the relative amplitude difference between each nano-fin for all wavelengths in the case of circularly polarized illumination, as each nano-fin is identical, and consequently, has the same size. We experimentally demonstrate this concept by measuring meta-axicons consisting of silicon nano-fins from the near-infrared to the visible spectrum, where silicon becomes intrinsically lossy (Supplementary Fig. S11). It is clearly observed that the sizes of the Bessel beam remain constant over the wavelength range of 532–800 nm.

## CONCLUSIONS

In summary, as a superior alternative to using conventional prism axicons or an objective paired with an annular aperture, we demonstrate high NA meta-axicons capable of generating Bessel beams of different orders in a single device in a much more efficient and compact way. The FWHM of $J_0$ and $J_1$ Bessel beams are shown to be as small as ~160 and 130 nm at the design wavelength $\lambda = 405$ nm. This size is maintained for an exceptionally large distance of $150\lambda$ (depth of focus). Their polarization is space-variant due to high NA. By tailoring the phase profile of the meta-axicons, the FWHMs of generated Bessel beams are made independent of the wavelength of incident light. These meta-axicons can be mass-produced with large diameter using today's industrial manufacturing (deep ultraviolet steppers). These properties show great promise in potential applications ranging from laser lithography and manipulation to imaging.

## CONFLICT OF INTEREST

The authors declare no conflict of interest.

## ACKNOWLEDGEMENTS

This work was supported in part by the Air Force Office of Scientific Research (MURI, grant# FA9550-14-1-0389), Charles Stark Draper Laboratory, Inc. (SC001-0000000959) and Thorlabs Inc. WTC acknowledges postdoctoral fellowship support from the Ministry of Science and Technology, Taiwan (104-2917-I-564-058). RCD is supported by a Charles Stark Draper Fellowship. AYZ thanks Harvard SEAS and A*STAR Singapore under the National Science Scholarship scheme. This work was performed in part at the Center for Nanoscale Systems (CNS), a member of the National Nanotechnology Coordinated Infrastructure (NNCI), which is supported by the National Science Foundation under NSF award no. 1541959. CNS is a part of Harvard University. We thank E. Hu for the supercontinuum laser (NKT 'SuperK').

1 Durnin J, Miceli JJ, Eberly JH. Diffraction-free beams. *Phy Rev Lett* 1987; **58**: 1499–1501.
2 Bouchal Z, Wagner J, Chlup M. Self-reconstruction of a distorted nondiffracting beam. *Opt Commun* 1998; **151**: 207–211.
3 Chen J, Ng J, Lin ZF, Chan CT. Optical pulling force. *Nat Photon* 2011; **5**: 531–534.
4 Dogariu A, Sukhov S, Jose Sáenz J. Optically induced 'negative forces'. *Nat Photon* 2013; **7**: 24–27.
5 Brzobohatý O, Čižmár T, Zemánek P. High quality quasi-Bessel beam generated by round-tip axicon. *Opt Express* 2008; **16**: 12688–12700.
6 Planchon TA, Gao L, Milkie DE, Davidson MW, Galbraith JA *et al.* Rapid three-dimensional isotropic imaging of living cells using Bessel beam plane illumination. *Nat Methods* 2011; **8**: 417–423.
7 Sun SL, Yang K-Y, Wang C-M, Juan T-K, Chen WT *et al.* High-efficiency broadband anomalous reflection by gradient meta-surfaces. *Nano Lett* 2012; **12**: 6223–6229.
8 Arbabi A, Horie Y, Bagheri M, Faraon A. Dielectric metasurfaces for complete control of phase and polarization with subwavelength spatial resolution and high transmission. *Nat Nanotechnol* 2015; **10**: 937–943.
9 Yu NF, Genevet P, Kats MA, Aieta F, Tetienne J-P *et al.* Light propagation with phase discontinuities: generalized laws of reflection and refraction. *Science* 2011; **334**: 333–337.
10 Huang LL, Chen XZ, Bai BF, Tan QF, Jin GF *et al.* Helicity dependent directional surface plasmon polariton excitation using a metasurface with interfacial phase discontinuity. *Light Sci Appl* 2013; **2**: e70.

11 Sun SL, He Q, Xiao SY, Xu Q, Li X *et al.* Gradient-index meta-surfaces as a bridge linking propagating waves and surface waves. *Nat Mater* 2012; **11**: 426–431.
12 Sun WJ, He Q, Sun SL, Zhou L. High-efficiency surface plasmon meta-couplers: concept and microwave-regime realizations. *Light Sci Appl* 2016; **5**: e16003.
13 Chen XZ, Huang LL, Mühlenbernd H, Li GX, Bai BF *et al.* Dual-polarity plasmonic metalens for visible light. *Nat Commun* 2012; **3**: 1198.
14 Arbabi A, Horie Y, Ball AJ, Bagheri M, Faraon A. Subwavelength-thick lenses with high numerical apertures and large efficiency based on high-contrast transmitarrays. *Nat Commun* 2015; **6**: 7069.
15 Khorasaninejad M, Chen WT, Devlin RC, Oh J, Zhu AY *et al.* Metalenses at visible wavelengths: Diffraction-limited focusing and subwavelength resolution imaging. *Science* 2016; **352**: 1190–1194.
16 Khorasaninejad M, Chen WT, Zhu AY, Oh J, Devlin RC *et al.* Multispectral chiral imaging with a metalens. *Nano Lett* 2016; **16**: 4595–4600.
17 Khorasaninejad M, Chen WT, Oh J, Capasso F. Super-dispersive off-axis meta-lenses for compact high resolution spectroscopy. *Nano Lett* 2016; **16**: 3732–3737.
18 Huang LL, Chen XZ, Mühlenbernd H, Zhang H, Chen SM *et al.* Three-dimensional optical holography using a plasmonic metasurface. *Nat Commun* 2013; **4**: 2808.
19 Huang YW, Chen WT, Tsai WY, Wu PC, Wang CM *et al.* Aluminum plasmonic multicolor meta-hologram. *Nano Lett* 2015; **15**: 3122–3127.
20 Zheng GX, Mühlenbernd H, Kenney M, Li GX, Zentgraf T *et al.* Metasurface holograms reaching 80% efficiency. *Nat Nanotechnol* 2015; **10**: 308–312.
21 Ye WM, Zeuner F, Li X, Reineke B, He S *et al.* Spin and wavelength multiplexed nonlinear metasurface holography. *Nat Commun* 2016; **7**: 11930.
22 Wang Q, Rogers ETF, Gholipour B, Wang C-M, Yuan GH *et al.* Optically reconfigurable metasurfaces and photonic devices based on phase change materials. *Nat Photon.* 2016; **10**: 60–65.
23 Ou J-Y, Plum E, Zhang JF, Zheludev NI. An electromechanically reconfigurable plasmonic metamaterial operating in the near-infrared. *Nat Nanotechnol* 2013; **8**: 252–255.
24 Karimi E, Schulz SA, De Leon I, Qassim H, Upham J *et al.* Generating optical orbital angular momentum at visible wavelengths using a plasmonic metasurface. *Light Sci Appl* 2014; **3**: e167.
25 Chen WT, Török P, Foreman MR, Liao CY, Tsai W-Y *et al.* Integrated plasmonic metasurfaces for spectropolarimetry. *Nanotechnology* 2016; **27**: 224002.
26 Khorasaninejad M, Crozier KB. Silicon nanofin grating as a miniature chirality-distinguishing beam-splitter. *Nat Commun* 2014; **5**: 5386.
27 Lin DM, Fan PY, Hasman E, Brongersma ML. Dielectric gradient metasurface optical elements. *Science* 2014; **345**: 298–302.
28 Hess O, Pendry JB, Maier SA, Oulton RF, Hamm JM *et al.* Active nanoplasmonic metamaterials. *Nat Mater* 2012; **11**: 573–584.
29 Aieta F, Genevet P, Kats MA, Yu NF, Blanchard R *et al.* Aberration-free ultrathin flat lenses and axicons at telecom wavelengths based on plasmonic metasurfaces. *Nano Lett* 2012; **12**: 4932–4936.
30 Gao L, Shao L, Chen B-C, Betzig E. 3D live fluorescence imaging of cellular dynamics using Bessel beam plane illumination microscopy. *Nat Protoc* 2014; **9**: 1083–1101.
31 Fahrbach FO, Simon P, Rohrbach A. Microscopy with self-reconstructing beams. *Nat Photon*. 2010; **4**: 780–785.
32 Brzobohatý O, Karásek V, Šiler M, Chvátal L, Čižmár T *et al.* Experimental demonstration of optical transport, sorting and self-arrangement using a 'tractor beam'. *Nat Photon.* 2013; **7**: 123–127.
33 Garcés-Chávez V, McGloin D, Melville H, Sibbett W, Dholakia K. Simultaneous micromanipulation in multiple planes using a self-reconstructing light beam. *Nature* 2002; **419**: 145–147.
34 Novitsky A, Qiu C-W, Wang HF. Single gradientless light beam drags particles as tractor beams. *Phys Rev Lett* 2011; **107**: 203601.
35 Yalizay B, Ersoy T, Soylu B, Akturk S. Fabrication of nanometer-size structures in metal thin films using femtosecond laser Bessel beams. *Appl Phys Lett* 2012; **100**: 031104.
36 Tseng ML, Wu PC, Sun S, Chang CM, Chen WT *et al.* Fabrication of multilayer metamaterials by femtosecond laser-induced forward-transfer technique. *Laser Photon Rev* 2012; **6**: 702–707.
37 Berry MV. The adiabatic phase and Pancharatnam's phase for polarized light. *J Mod Opt* 1987; **34**: 1401–1407.
38 Gori F. Measuring Stokes parameters by means of a polarization grating. *Opt Lett* 1999; **24**: 584–586.
39 Luo WJ, Xiao SY, He Q, Sun SL, Zhou L. Photonic spin Hall effect with nearly 100% efficiency. *Adv Opt Mater* 2015; **3**: 1102–1108.
40 Huang LL, Chen XZ, Mühlenbernd H, Li GX, Bai BF *et al.* Dispersionless phase discontinuities for controlling light propagation. *Nano Lett* 2012; **12**: 5750–5755.
41 Devlin RC, Khorasaninejad M, Chen WT, Oh J, Capasso F. Broadband high-efficiency dielectric metasurfaces for the visible spectrum. *Proc Natl Acad Sci USA* 2016; **113**: 10473–10478.
42 Lalanne P, Astilean S, Chavel P, Cambril E, Launois H. Blazed binary subwavelength gratings with efficiencies larger than those of conventional échelette gratings. *Opt Lett* 1998; **23**: 1081–1083.
43 Bomzon Z, Gu M, Shamir J. Angular momentum and geometrical phases in tight-focused circularly polarized plane waves. *Appl Phys Lett* 2006; **89**: 241104.
44 Lalithambigai K, Suresh P, Ravi V, Prabakaran K, Jaroszewicz Z *et al.* Generation of sub wavelength super-long dark channel using high NA lens axicon. *Opt Lett* 2012; **37**: 999–1001.
45 Novitsky AV, Novitsky DV. Negative propagation of vector Bessel beams. *J Opt Soc Am A Opt Image Sci Vis* 2007; **24**: 2844–2849.
46 Leach J, Gibson GM, Padgett MJ, Esposito E, McConnell G *et al.* Generation of achromatic Bessel beams using a compensated spatial light modulator. *Opt Express* 2006; **14**: 5581–5587.
47 Escuti MJ, Kim J, Kudenov MW. Controlling light with geometric-phase holograms. *Opt Photon News* 2016; **27**: 22–29.
48 Song L, Lessard RA, Galarneau P. Diffraction efficiency of a thin amplitude-phase holographic grating: a convolution approach. *J Mod Opt* 1990; **37**: 1319–1328.



Supplementary Information for this article can be found on the *Light: Science & Applications*' website (http://www.nature.com/lsa).